Variation of Atmospheric Stabilities and Their Relationship with Gravity Wave Dissipation and Turbulence

Fan Yang and Alan Z. Liu
Center for Space and Atmospheric Research and Department of Physical Sciences
Embry-Riddle Aeronautical University, Daytona Beach, FL, USA

CEDAR 2018

Email: yangf1@my.erau.edu

Abstract: The square of buoyancy frequency N^2 and the Richardson number Ri are commonly used to characterize the convective and dynamic stabilities of the atmosphere, respectively. We report a detailed analysis of these parameters based on high-resolution temperature and horizontal wind measurement made with Na Lidar at Andes Lidar Observatory (30.2˚S,70.7˚W) and compared with results from earlier measurement made at Maui, HI, USA (20.7˚N, 156.2˚W). Uncertainties and biases of the instability probabilities due to photon noise are analyzed, and the biases are subtracted from the measured probabilities. The seasonal and altitudinal variations of the instabilities probabilities show the combined effect of seasonal variation of background atmosphere and wave activities. When compared with gravity heat flux, turbulence heat flux, and thermal diffusion, we found that their variations are opposite (more dissipation in more stable atmosphere) but can be explained by gravity wave intermittency. This has implications for parameterizing wave effects in models.

Introduction

In the upper mesosphere, atmospheric instabilities are key dynamical processes that are responsible for dissipation of gravity waves and their energy and momentum deposition to the background atmosphere. Two main instability processes are the convective and dynamic (shear) instabilities. The atmosphere becomes convectively unstable when $N^2<0$ and becomes dynamically unstable when $0<Ri<1/4$, where N is the buoyancy frequency related to vertical temperature gradient and Ri is the Richardson number related to vertical gradient of horizontal wind.

In this study, we examine the structure and seasonal variations of convective and dynamic (shear) instabilities in the upper mesosphere by using 3-year high-resolution wind and temperature data obtained with the Na Lidar at Andes Lidar Observatory (30.2˚S,70.7˚W) and Maui, HI, USA (20.7N, 156.2W). Even with high-quality lidar data, accurate measurement of N^2 and Ri requires careful analysis of their uncertainties and biases arising from errors in temperature and horizontal wind due to photon noise in the measurement process. We present here

1. a detailed analysis of the bias of measured probabilities of instabilities, $P(N^2<0)$, $P(S>40)$ and $P(0<Ri<1/4)$,
2. seasonal and vertical variations of these probabilities,
3. and the relation between the instability parameters and turbulence.

Data and Stability Parameters

1. Data Summary

Andes Lidar Observatory, Cerro Pachón, Chile (30.3S, 70.7W) (2014-2018), 1000 hr, temperature every month, no horizontal wind in May, Aug & Sep

Maui, HI, USA (20.7N, 156.2W), 250 hr, in 7 calendar months (2001-2005).

The number of total observation nights for ALO are listed in the right table. The numbers in parenthesis indicate the number of nights when horizontal wind is available. The total nights in each calendar month for both ALO and Maui are shown in the table below.

ALO	
Month	Total nights
May, 2014	3 (0)
Aug-Sep, 2014	16 (0)
Jan-Feb, 2015	16 (6)
Apr, 2015	13 (8)
July, 2015	10 (10)
Oct-Nov, 2015	8 (7)
Feb-Mar 2016	16 (16)
June 2016	6 (6)
Oct-Nov 2016	17 (17)
Apr-May 2017	8 (8)
Nov-Dec 2017	20 (20)
Jan 2018	12 (12)
Total	122 (87)

	1	2	3	4	5	6	7	8	9	10	11	12
ALO	26 (26)	7 (7)	14 (14)	20 (20)	5 (0)	6 (6)	11 (11)	4 (0)	7 (0)	10 (10)	15 (15)	11 (11)
Maui	6 (6)	0 (0)	3 (3)	5 (5)	3 (3)	0 (0)	9 (9)	4 (4)	0 (0)	6 (6)	1 (1)	0 (0)

2. Stability Parameters

$$N^2 = \frac{g}{T}\left(\frac{g}{C_p} + \frac{dT}{dz}\right) \quad S = \sqrt{(du/dz)^2 + (dv/dz)^2} \quad Ri = N^2/S^2$$

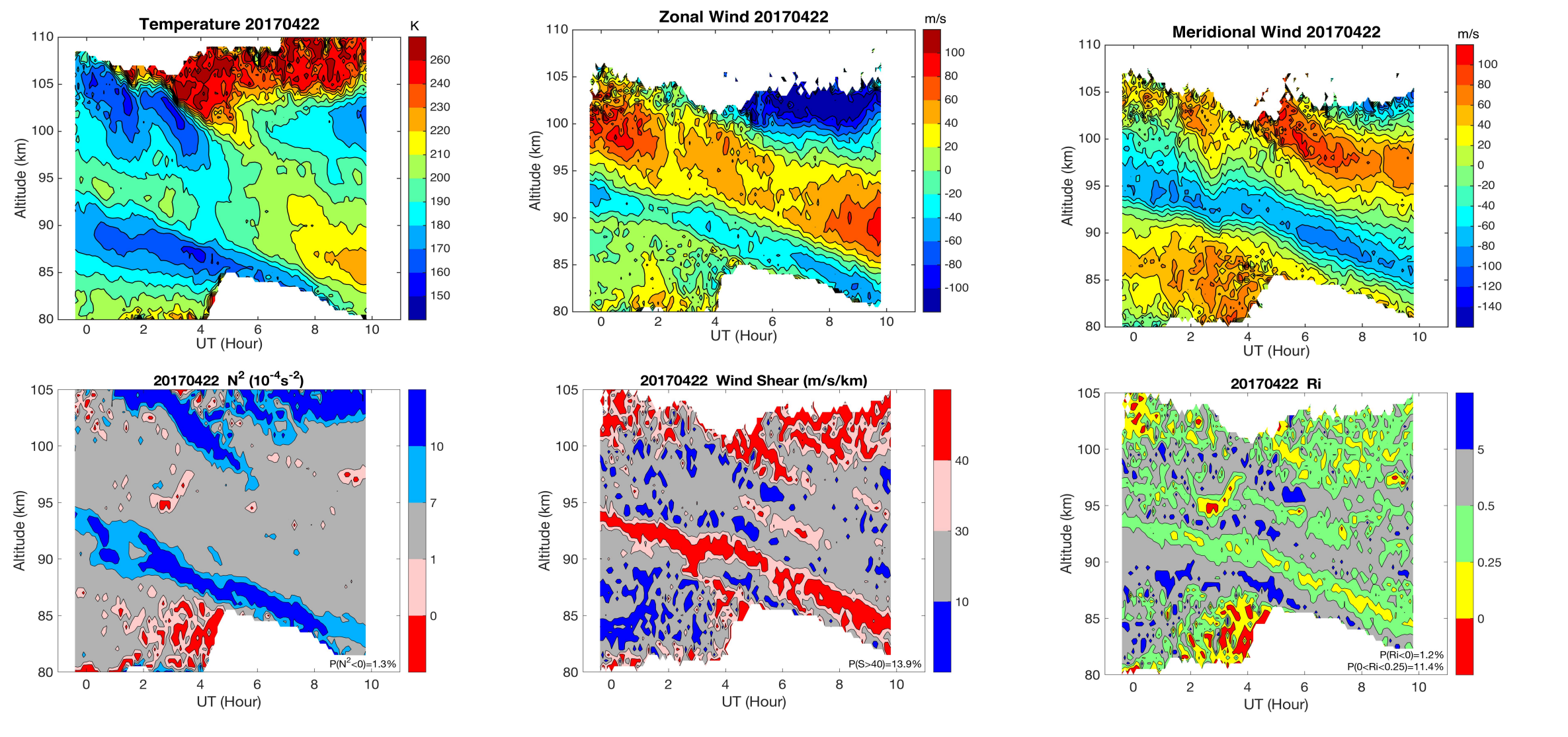

Figure 1. Temperature and horizontal wind on April 22nd, 2017 and corresponding stability parameters and wind shear.

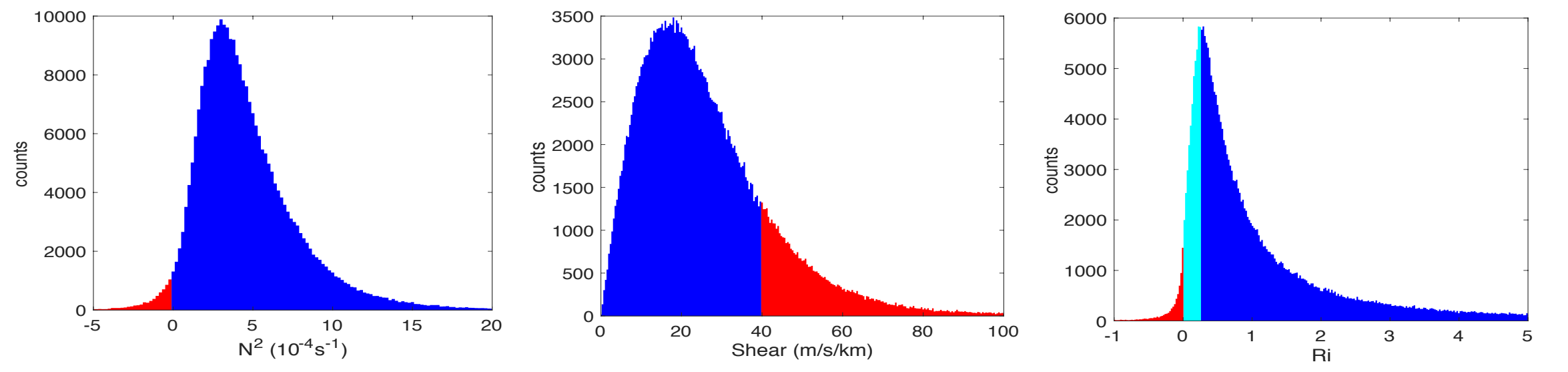

Figure 2. Histograms of N^2 , S and Ri from all measurements between 85-100 km at ALO. Red in N^2 indicates convective instability ($N^2<0$). Red in S indicates large shear (S>40 m/s/km). Light blue indicates dynamic instability (0<Ri<0.25).

Bias correction

- Probability of convective instability $P(N^2<0)$ is defined as the fraction of measurements with $N^2<0$. Probability of large shear P(S>40) is defined as the fraction of measurements with S>40 m/s/km. And probability of dynamic instability P(0<Ri<0.25) is the fraction of measurements with 0<Ri<0.25
- Photon noise creates errors in measured temperature and wind. These errors propagate to N^2 and Ri and then to $P(N^2<0)$, P(S>40) and P(0<Ri<0.25). There are both random errors and biases in $P(N^2<0)$, P(S>40) and P(0<Ri<0.25).
- Monte-Carlo simulations are used to estimate these errors and biases. Random Gaussian errors are added to temperature and wind to obtain the corresponding distributions of $P(N^2<0)$, P(S>40) and P(0<Ri<0.25). The standard deviations and differences in mean values are the random errors and biases, respectively.
- Simulations show that the random errors are about 1~2% for P(N2<0), 10~40% for P(S>40) and -5~10% for P(0<Ri<0.25). The biases are not negligible but can be corrected.

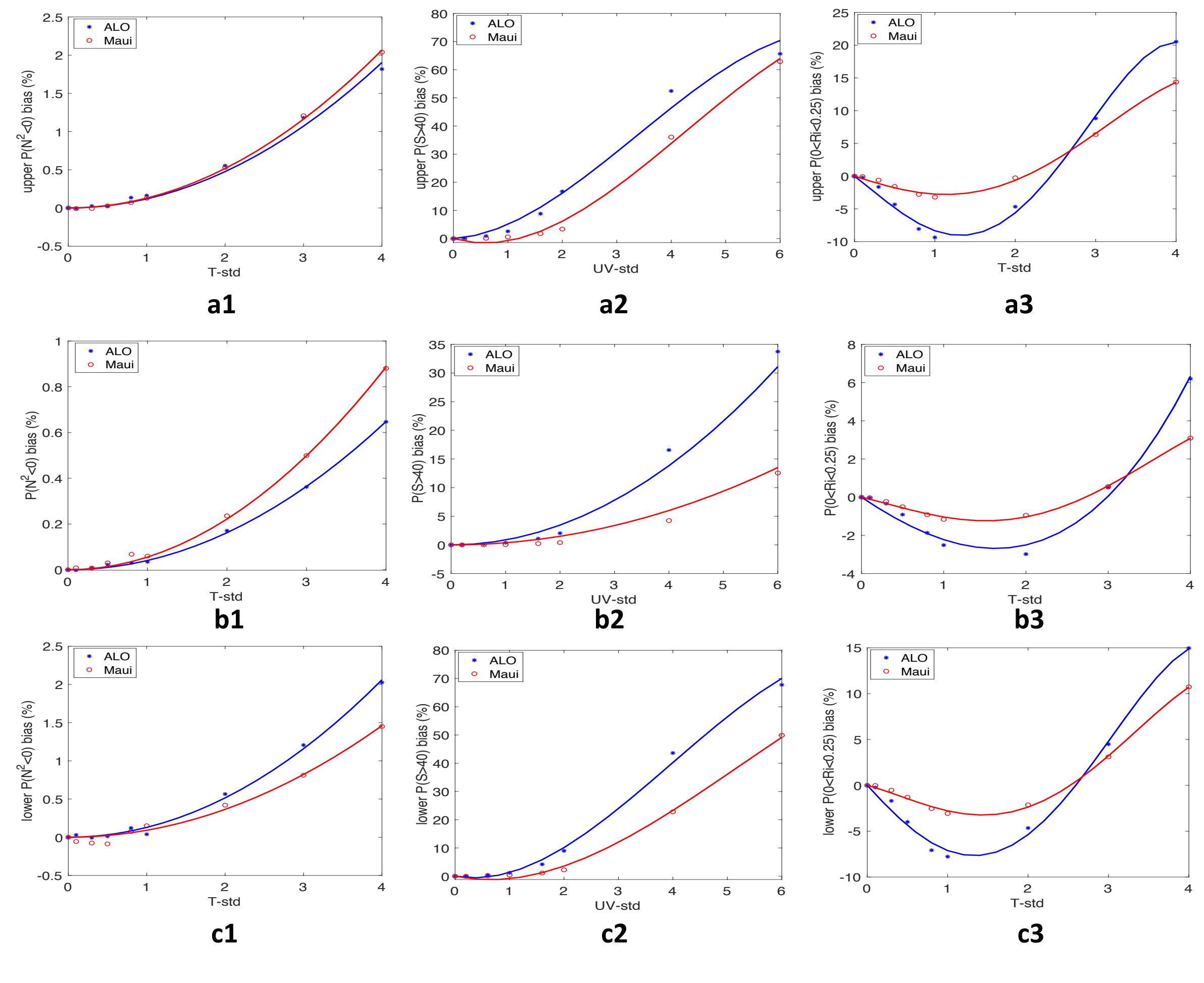

a1 a2 a3
b1 b2 b3
c1 c2 c3

Figure 3. Biases of $P(N^2<0)$, P(S>40) and P(0<Ri<0.25). as functions of temperature and wind errors and probability values. a1~a3 are for altitude of 98-108km, b1~b3 are for altitude of 88-98km and c1~c3 are for altitude of 78-88km.

Stabilities

$P(N^2<0)$, P(S>40) and P(0<Ri<0.25) are calculated at 1.0 km vertical resolution for all measurement within each calendar month. Biases are corrected based on the mean rms errors in temperature and horizontal wind.

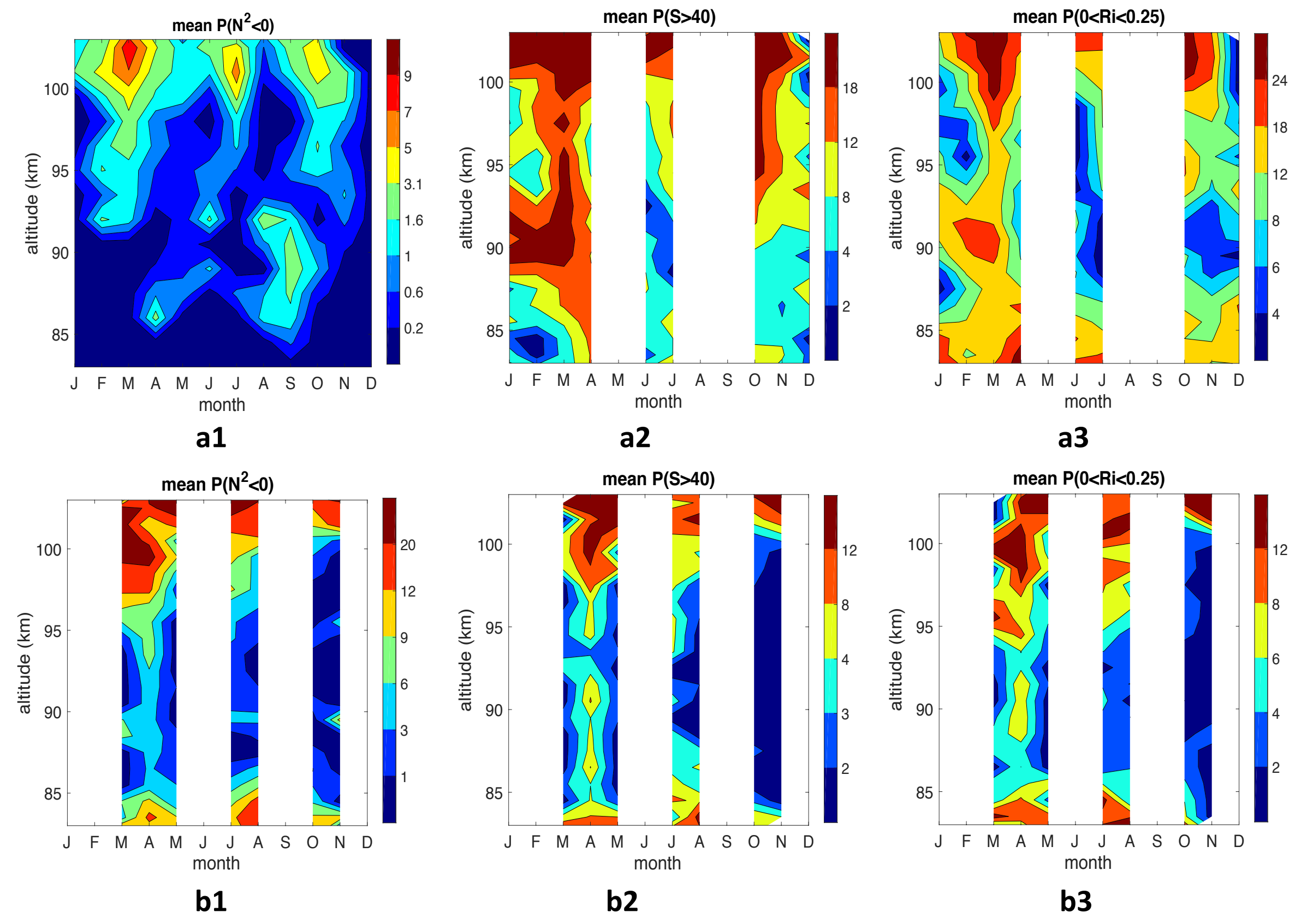

a1 a2 a3
b1 b2 b3

Figure 4. Seasonal and altitudinal distributions of $P(N^2<0)$, P(S>40) and P(0<Ri<0.25 for ALO (a1~a3) and Maui (b1~b3).

Stabilities and GW

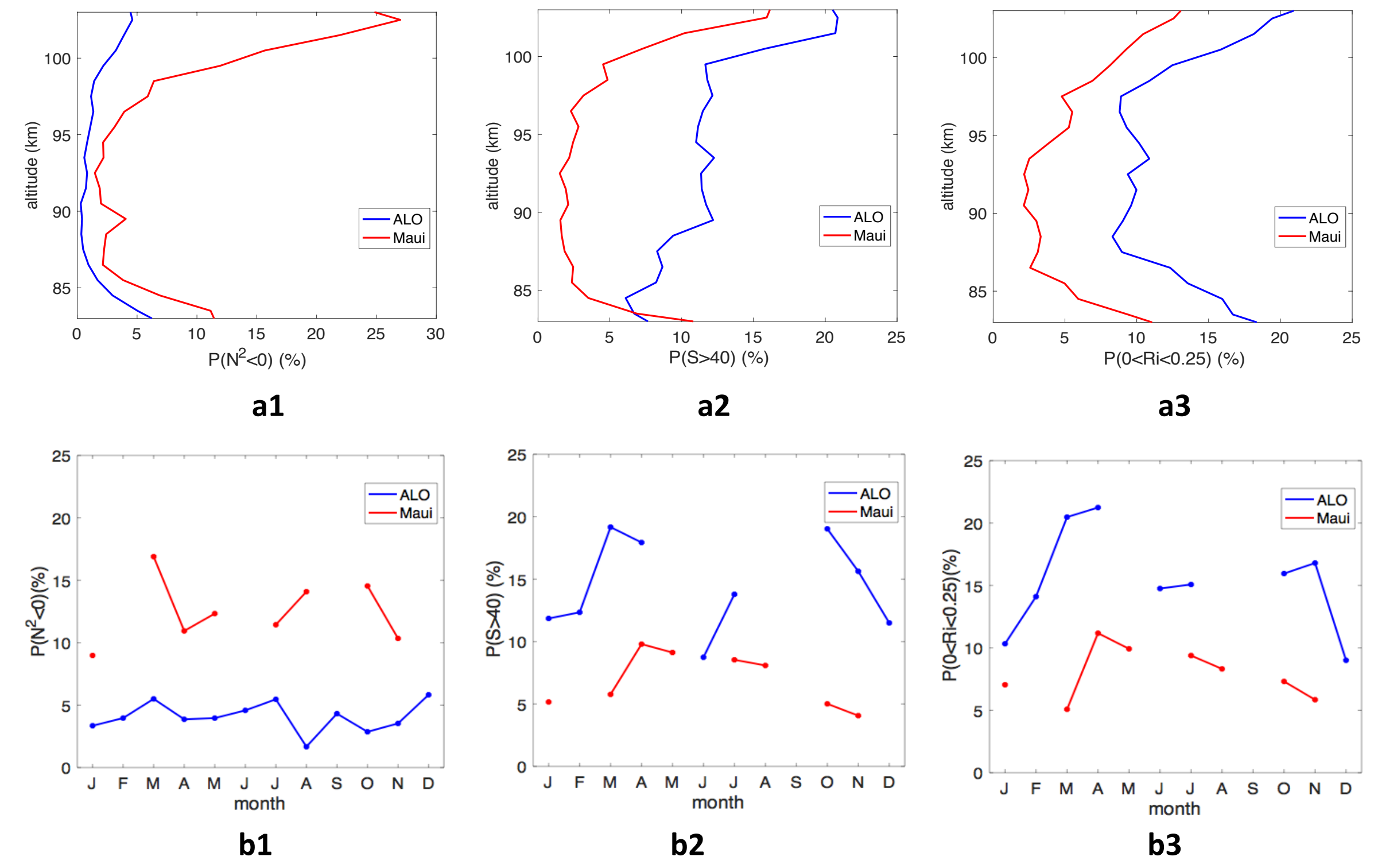

a1 a2 a3
b1 b2 b3

Figure 5. Altitudinal and seasonal average of $P(N^2<0)$, P(S>40) and P(0<Ri<0.25) for ALO and Maui (b1~b3).

Compared with Maui, $P(N^2<0)$ is lower (~1%) while P(0<Ri<0.25) is higher (~10%) at ALO — Much higher convective instability probability in Maui and much higher dynamic instability probability in Chile.

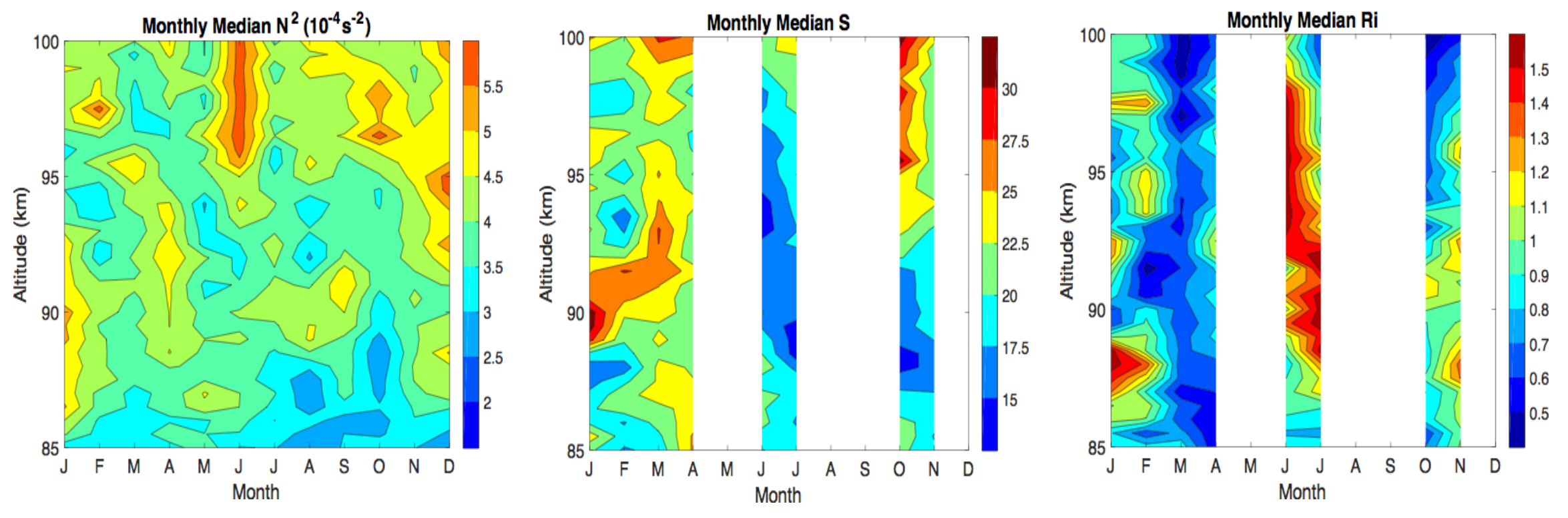

Figure 6 . Seasonal and altitudinal distributions of medians of N^2, S and Ri at ALO.

In Figure 6, S is large in March and Ri is small, so P(S>40) and P(0<Ri<0.25) as shown in Figure 4-a2,a3 are high. June/July are just the opposite.

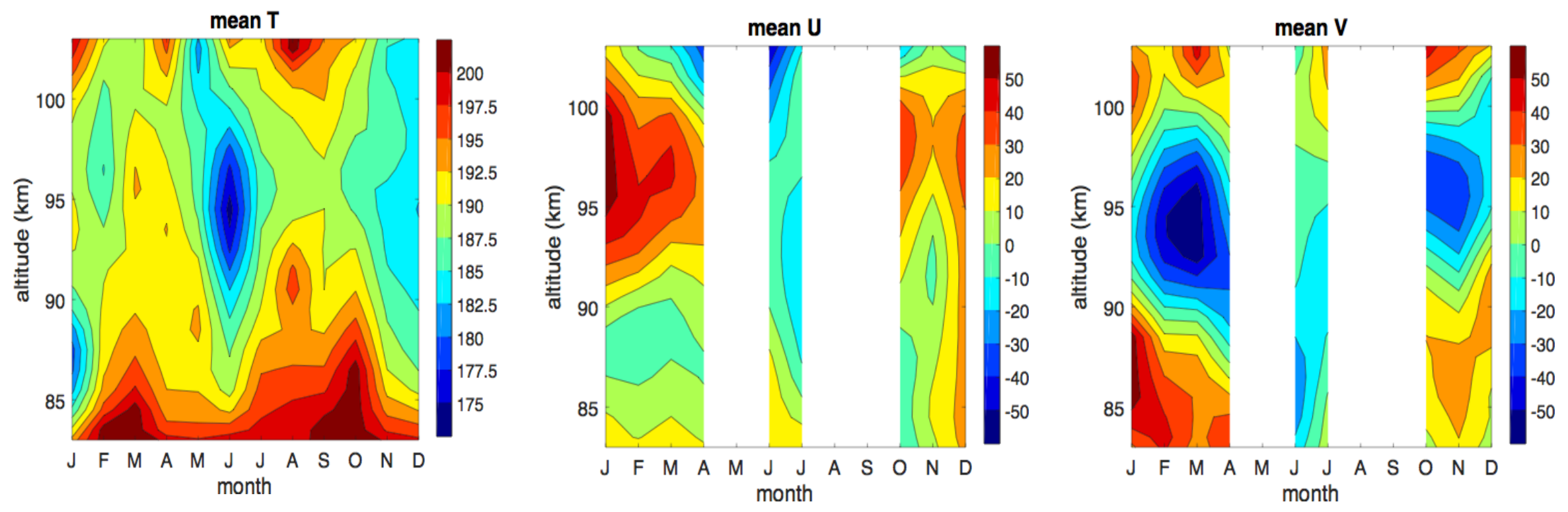

Figure 7 . Seasonal and altitudinal distributions of temperature, zonal wind and meridional wind at ALO.

In Figure 7, S is large in March and Ri is small, so P(S>40) and P(0<Ri<0.25) as shown in Figure 4-a2,a3 are high. June/July are just the opposite. In Figure 6, there 3 parameters are calculated from high resolution data, not from mean temperature and wind. So seasonal variations of these parameters are largely controlled by background, even we used data with GWs effects.

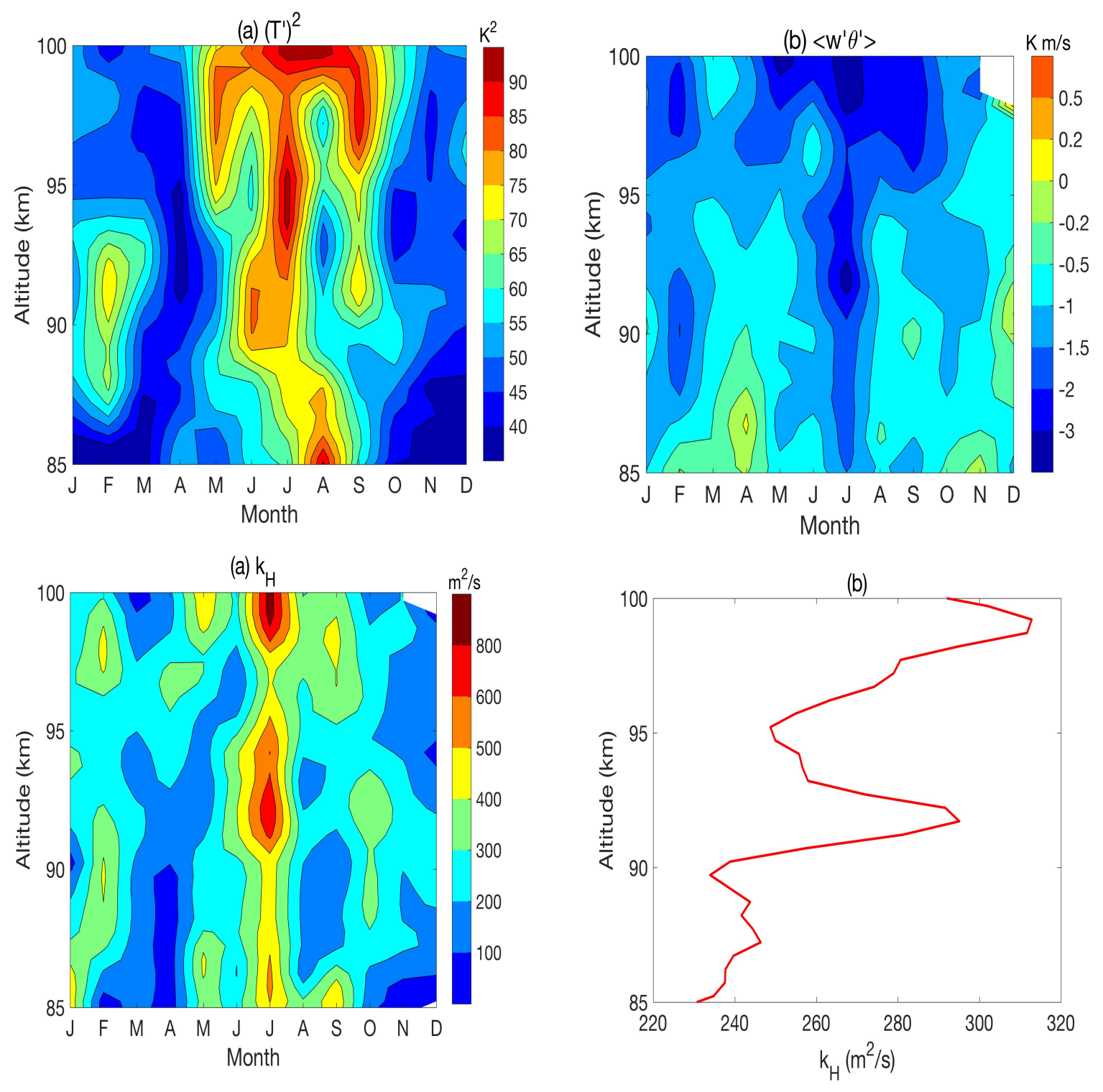

$$K_H \approx -\frac{2g}{\bar{\theta}N^2(1-2\eta)}\overline{w'\theta'}$$

Fritts and Dunkerton 1985,
Liu, H-L, 2000
Liu, A. Z. 2009
Guo and Liu JGR 2018

Figure 8. Seasonal and altitudinal GW variance, heat (enthalpy) flux and effective thermal diffusivity at ALO.

Stabilities and Turbulence

Figure 8 shows that GW is strong in June/July (winter), which is most likely due to mountain waves. GW heat flux and effective thermal diffusivity indicate GW dissipation. Strong GW dissipation in winter corresponds to low instability probability;weak dissipation in March corresponds to high instability probability. Wave dissipation is controlled by both wave source, amplitude, and background stability. Stability alone is not sufficient as an indication of wave dissipation.

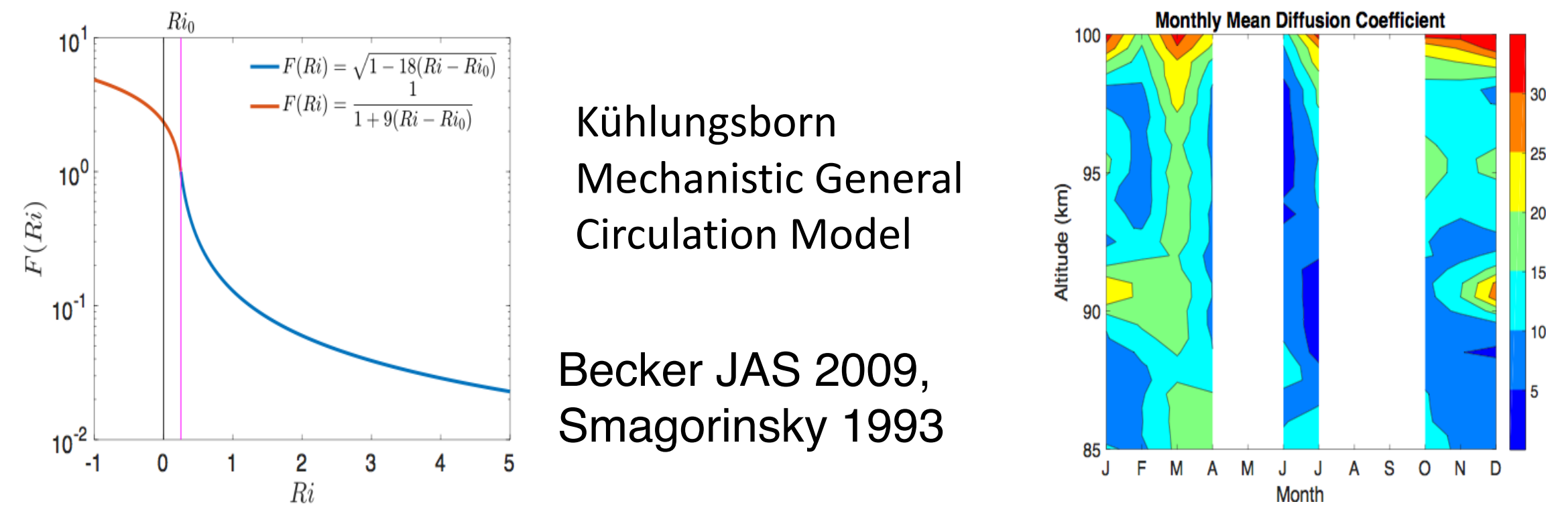

Kühlungsborn
Mechanistic General
Circulation Model

Becker JAS 2009,
Smagorinsky 1993

Figure 9. Seasonal and altitudinal eddy diffusion based on measured S and Ri at ALO and Becker's formula.

Figure 9 shows eddy diffusion K is smallest in winter, and largest in March, which is opposite to the measured wave dissipation (heat flux) shown in Figure 8. Parameterizing eddy diffusion based on stability may not be sufficient to properly represent the wave dissipation.

Turbulence plays a major role in the upper atmosphere through constituents and heat transport. Guo et al. (JGR 2017) showed that the Na wind/temperature lidar at ALO is capable of detecting turbulence-scale perturbations and providing direct measurements of the eddy heat flux and thermal diffusion coefficient. We apply this same method to study the relationship between stabilities and turbulence.

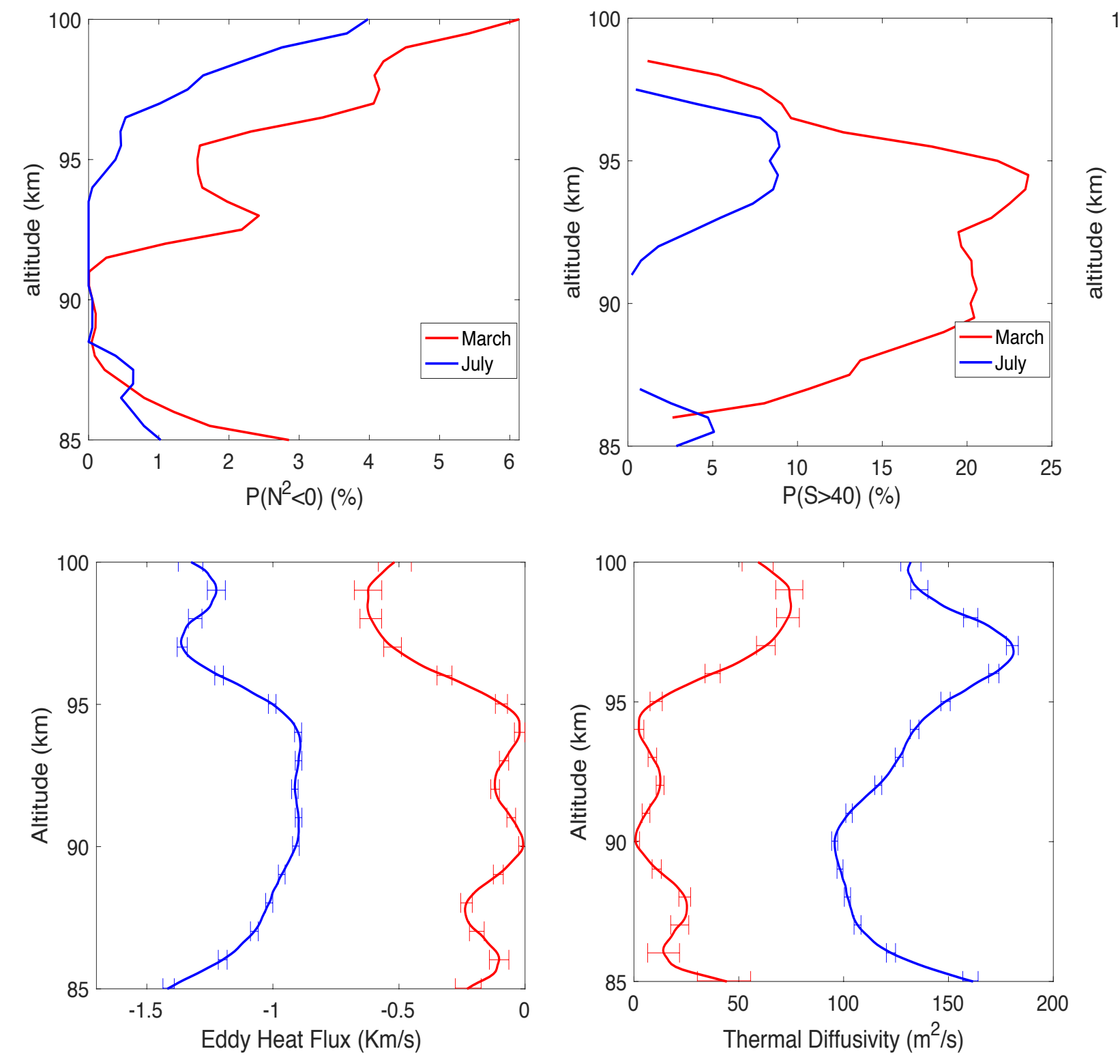

Figure 10. Instability probabilities and turbulence vertical heat flux and thermal eddy diffusion of ALO in March (red) and July (blue).

In general, probabilities for convective and dynamic instabilities are higher in March but turbulence flux and thermal diffusion are larger in July. The latter is consistent with result in Figure 8. In both March and July, the vertical structures of thermal diffusivity are consistent with those of the corresponding P(0<Ri<0.25), indicating a correlation between turbulence diffusion and dynamic instability.

Summary

- Na Lidar Measurement is uniquely capable for MLT stability analysis
- Uncertainties and biases of $P(N^2<0)$, P(S>40) and P(0<Ri<0.25) are derived and biases are corrected
- Seasonal variations of stability parameters are largely controlled by background
- ALO measurements show (compared with Maui) very low $P(N^2<0)$ ~1% and high P(0<Ri<0.25) ~10%.
- GW and dissipation and turbulence are strongest in June/July (probably due to MWs) though shear is weak.
- March is dynamically most unstable while GW activity is weakest
- June/July: large intermittency + stable background — small P(0<Ri<0.25) + strong GW dissipation and turbulence
  March: small intermittency + and less stable background — high P(0<Ri<0.25) + weak GW dissipation and turbulence
- Stability criteria may not be sufficient for parameterization of eddy diffusion. Wave intermittency is another important factor.

Acknowledgements: This work is supported by NSF grants AGS-1136208, AGS-1229085 and AGS-1136278. Data used in this analysis was taken mostly by Dr. Fabio Vargas.